NEW PICTURE OF PHASE EQUILIBRIA IN THE Cu-As-Se SYSTEM AND THERMODYNAMIC PROPERTIES OF TERNARY COMPOUNDS

[a]Leyla F. Mashadiyeva*, [a]Albina N. Poladova, [b]Ziver T. Hasanova, [a]Bilgeyis A. Ismayilova, [b]Eldar I. Ahmadov, [b]Yasin I. Jafarov, [c]Yusif A. Yusibov, [a,b,d]Mahammad B. Babanly

[a]Institute of Catalysis and Inorganic Chemistry, Baku, Azerbaijan
[b]Baku State University, Baku, Azerbaijan
[c]Ganja State University, Ganja, Azerbaijan
[d]Azerbaijan State University of Economics Baku, Azerbaijan
**leylafm76@gmail.com*

Received 13.07.2024
Accepted 28.09.2024

Abstract. *A new complete picture of phase equilibria in the Cu-As-Se system was obtained by experimentally studying carefully crystallized alloys by prolonged thermal annealing using differential thermal analysis and powder X-ray diffraction methods, as well as considering information found in the literature. The liquidus surface projection, isothermal section at 300 K and some vertical sections of the phase diagram are presented and discussed. The types and coordinates of nonvariant and monovariant phase equilibria are determined. It is established that the liquidus surface consists of 15 regions corresponding to the primary crystallization of three initial components, seven binary and five ternary compounds. The presented phase diagram reflects the compounds Cu_3AsSe_4, Cu_3AsSe_3, $Cu_7As_6Se_{13}$, $CuAsSe_2$ and CuAsSe, which can be considered as synthetic analogues of natural copper-arsenic minerals. The ternary compounds $Cu_6As_4Se_9$ and $Cu_4As_2Se_5$, indicated in the literature, have not been confirmed by us. The thermodynamic properties of ternary copper-arsenic selenides were studied using the EMF method with the solid electrolyte $Cu_4RbCl_3I_2$. From the EMF measurement data in the corresponding three-phase regions, linear equations of the temperature dependence of the EMF were obtained, from which partial thermodynamic functions of copper in the alloys were calculated. Based on these data and the solid-phase equilibrium diagram of the Cu-As-Se system, using the corresponding thermodynamic functions of copper, As_2Se_3, AsSe and Cu_3AsSe_4, the standard Gibbs free energy of formation and the enthalpy of formation, as well as the standard entropy of the ternary compounds Cu_3AsSe_3, $Cu_7As_6Se_{13}$, $CuAsSe_2$ and CuAsSe, were calculated.*

Key words: *phase diagram; liquidus surface projection; polythermal section; solidphase equilibria; Cu_2Se-As_2Se_3 system, standard thermodynamic functions of formation, Cu_3AsSe_3, $Cu_7As_6Se_{13}$, $CuAsSe_2$, CuAsSe.*
DOI: 10.32737/2221-8688-2025-3-310-328

1. Introduction

Ternary copper chalcogenides are functional compounds due to their unique physical and chemical properties. They are widely used in many different domains, including catalysis, electronics, optoelectronics, and photoelectronics [1–8]. The results of numerous studies show the possibility of their application in alternative energy devices and other areas of high technology [9-13]. Many of these compounds have mixed ion-electron conductivity, making them very promising in developing photoelectrode materials and ion-selective sensors [14-16].

Copper-arsenic chalcogenide systems Cu-As-X (X=S, Se) are of great interest to researchers. Ternary compounds and glassy alloys of these systems are valuable functional materials possessing semiconductor, photoelectric, optical and other practically important properties [17-25]. On the other hand, many known ternary compounds formed in Cu-As-S(Se) systems occur in nature as minerals and are of considerable interest for the study of the Earth's geochemistry [26-28]. Thus, synthetic analogues of copper minerals are used in scientific research to study and understand the properties and characteristics of these minerals,

such as their structure, thermophysical properties, magnetic properties, etc.

It is known that when developing new complex materials, information on phase equilibria and thermodynamic characteristics of the corresponding systems is of great importance, as they are the basic data for developing methods for synthesis, alloying, and growing single crystals with specified characteristics [29-31]. Earlier, in a number of works [32-44], we conducted similar comprehensive studies of complex systems based on copper chalcogenides.

In our recently published work [45], a new picture of phase equilibria in the Cu-As-S system was obtained and refined data on the standard thermodynamic functions of formation and the standard entropy of the ternary phases formed in it were obtained. This work aimed to receive a new, mutually consistent set of data on phase equilibria and thermodynamic properties of the Cu-As-Se system, which constitute the scientific basis for developing the phases formed in them.

Our analysis of the available literature data showed that the Cu-As-Se system has been studied in numerous works. However, a reliable picture of phase equilibria in this system has not been obtained to date. This concerns, first of all, data on the quasi-binary section Cu_2Se-As_2Se_3. The known versions of the T-x diagram of this section differ significantly from each other both in the number and composition of ternary compounds, and in the temperatures and nature of their melting.

The works [46, 47] summarize the results of earlier studies (before the 1990s) of phase equilibria and characteristics of ternary phases in the Cu–As–Se system. Later, Cohen et al. [48] presented new data on phase equilibria in this system, which diverge from the already published results. In particular, the authors' phase diagram only contained the first two ternary compounds: Cu_3AsSe_4, $CuAsSe_2$, Cu_3AsSe_3, and $Cu_6As_4Se_9$, which were reported in the literature. Regretfully, Cohen et al. [48] did not compare their data to those from other sources.

Therefore, a comparison of the existing data reveals that no trustworthy image of phase equilibria in the Cu–As–Se system has yet to be established, even though several polythermal sections have been explored. The discrepancy in the literature data on phase equilibria of this system, in our opinion, is largely due to the tendency of alloys to glass formation and the complexity of their crystallization and achievement of an equilibrium state.

Copper-arsenic selenide crystal structure has been investigated in several publications [49–52]. Table 1 presents crystallographic data for the ternary compounds of the Cu-As-Se system indicated in the literature.

Table 1. Types and parameters of crystal lattices of ternary compounds of the Cu-As-Se system

Compound	Structure, Sp.gr., lattice parameters; Å	Ref.
α-Cu_3AsSe_4	Cubic, a=5.535	[49]
β-Cu_3AsSe_4	Tetragonal, I-42m, a = 5.53, c = 10.83	[49]
$CuAsSe_2$	Monoclinic, a = 5.117, b = 12.293, c = 9.464, β = 98.546	[50]
$Cu_4As_2Se_5$	Rhombohedral, R3, a = 14.0401, c = 9.6021	[50]
Cu_3AsSe_3	Cubic, Pm-3m, a = 5.758	[51]
$Cu_7As_6Se_{13}$	Hexagonal, R3, a = 14.025, c = 9.61, γ = 120	[52]

As was indicated above, the previously presented phase diagrams of the main quasi-binary section Cu_2Se-As_2Se_3 of the Cu-As-Se system are contradictory (a detailed literature analysis was conducted in [53]). Therefore, in [53] this section was re-investigated by us and its refined phase diagram was constructed. It is shown that this system is quasi-binary and is characterized by the formation of ternary compounds Cu_3AsSe_3 and $CuAsSe_2$, which melt with decomposition according to peritectic reactions (Fig. 1). In [53] we also have presented a new picture of phase equilibria in the Cu_2Se-Cu_3AsSe_4-As_2Se_3 subsystem of the Cu-As-Se system. A projection of the liquidus surface of the Cu_2Se-Cu_3AsSe_4-As_2Se_3 system, an isothermal section at 500 K, and some vertical sections of the phase diagram were constructed. The fields of primary crystallization of all seven phases of the studied system, as well as types and

coordinates of invariant and monovariant phase equilibria are determined. The presented phase diagram reflects four ternary copper-arsenic selenides Cu_3AsSe_4, Cu_3AsSe_3, $Cu_7As_6Se_{13}$, and $CuAsSe_2$.

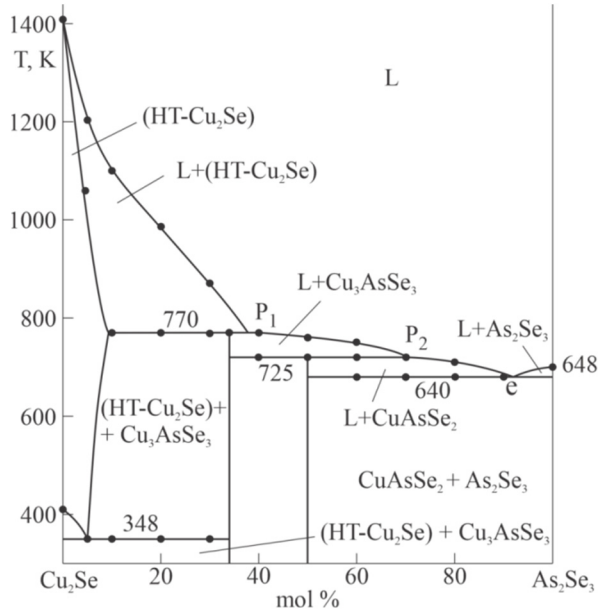

Fig. 1. Quasi-binary system Cu_2Se-As_2Se_3 [53]

Apart from the aforementioned subsystem, we have previously examined two more subsystems of the Cu-As-Se system (Fig. 2): Cu–Cu_2Se–As [54] and Cu_2Se–Cu_3AsSe_4–Se [55]. Using differential thermal analysis and X-ray structural analysis methods, informative graphs were constructed describing these subsystems, a number of polythermal sections and an isothermal section of the phase diagram at 300 K, as well as a projection of the liquidus surface. Using the EMF approach with solid electrolyte, we also evaluated in [55] the standard thermodynamic functions of formation and the standard entropy of the Cu_3AsSe_4 compound.

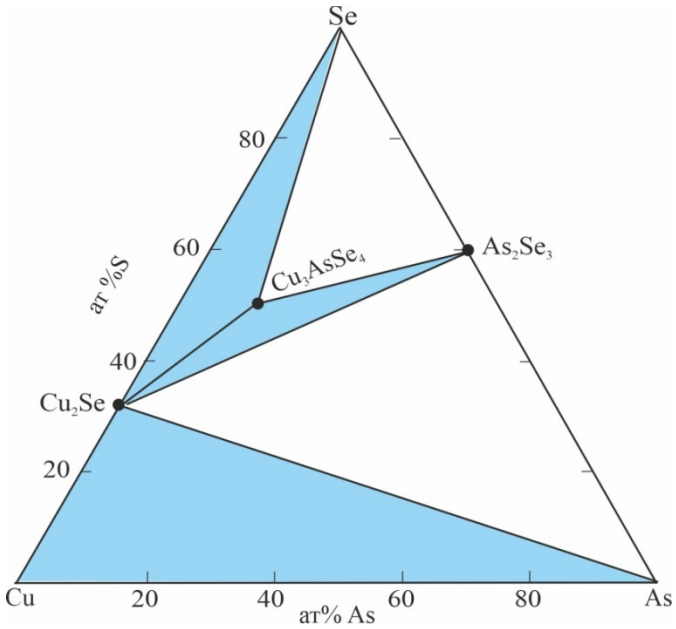

Fig. 2. Studied subsystems of the Cu-As-Se system [53-55]

Phase equilibria in the Cu-Se, As-Se, and Cu-As boundary binary components of the Cu-As-Se system have been thoroughly examined and are regarded as very trustworthy [56] (Fig. 3).

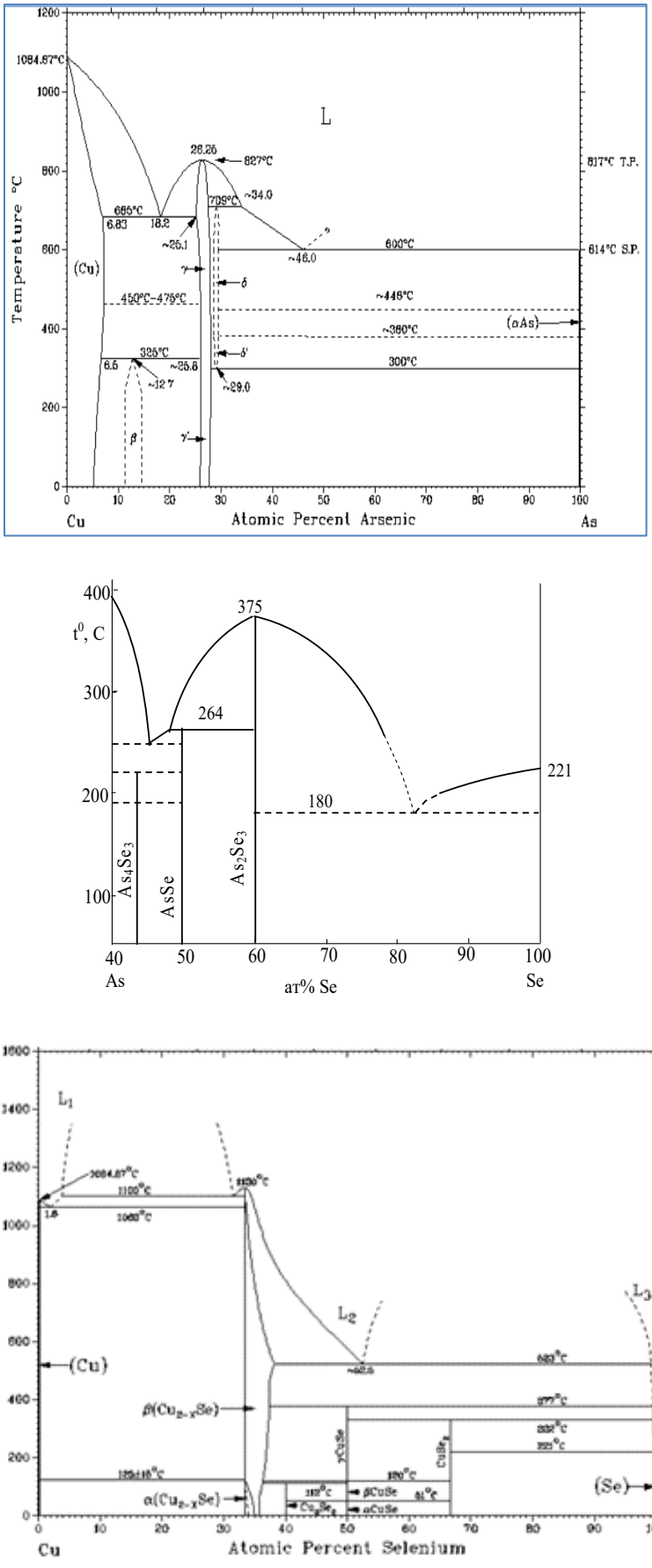

Fig. 3. Phase diagrams of the Cu-Se, As-Se and Cu-As systems [56]

2. Experimental part

2.1. Starting materials

Highly pure copper granules (Cu-00029; 99.9999%), arsenic pieces (As-00004; 99.9999%), and selenium granules (Se-00002; 99.999%) from Evochem Advanced Materials GmbH (Germany) were used for synthesis.

2.2. Synthesis

CuSe, $CuSe_2$, CuAs, AsSe and As_2Se_3 binary compounds were initially synthesized by direct interaction of stoichiometric amounts of the corresponding simple substances in evacuated (~10^{-2} Pa) and sealed silica ampoules. Synthesis of copper selenides was carried out in a two-zone inclined furnace. The temperature of the lower "hot" zone was 1420 K, and the upper "cold" zone was 900 K, which is slightly lower than the boiling point of selenium (958 K). Taking into account the incongruent melting of the CuSe and CuSe2 compound, after the fusion of the components at ~900 K, the ampoule was slowly cooled to 700 K, and annealed at this temperature for 500 hours. The identity of the synthesized copper selenides was verified by differential thermal analysis (DTA) and powder X-ray Diffraction (XRD) technique.

Pieces of elemental arsenic stored in an evacuated ampoule and without an oxide film were used for the synthesis of arsenic selenides. Elemental arsenic was weighed last and quickly for literally 2-3 minutes in order to minimize the likelihood of its oxidation. Arsenic selenides synthesized by fusion upon cooling solidified in the form of homogeneous glasses. Considering the difficulty of their crystallization, glassy AsSe and As_2Se_3 were used in the preparation of Cu-As-Se alloys.

To study phase equilibria, we synthesized stoichiometric composition of the known ternary compounds (Cu_3AsSe_4, Cu_3AsSe_3, $Cu_7As_6Se_{13}$, $CuAsSe_2$, CuAsSe, $Cu_6As_4Se_9$, $Cu_4As_2Se_5$) and alloys of some isopleth sections. When preparing the alloys, we took into account the results of our previous works and focused on the Cu_2Se-As_2Se_3-As and Cu_3AsSe_4-As_2Se_3-Se composition regions, which we had not previously considered (Fig. 2). Syntheses of ternary alloys were carried out by the interaction of pre-synthesized binary compounds and elementary components, also under vacuum conditions.

Considering the tendency of Cu-As-Se alloys to form glasses [57, 58], when preparing samples from the region of glass formation and its surroundings, we paid special attention to the complete crystallization of glasses and achieving an equilibrium state. The cast samples obtained by cooling the melts were subjected to long-term stepwise annealing. Cast alloys prepared by fusing the initial binary and some ternary compounds, as well as a glassy alloy of stoichiometric composition As_2Se_3 and elemental selenium, were subjected to thermal annealing at temperatures slightly below the solidus (500-600 K) for 2000-3000 h. As a result, we were able to obtain completely crystallized alloys.

2.3. Analysis

DTA and XRD techniques were employed to analyze both starting compounds and alloys. Thermal analysis of the equilibrated alloys was carried out using a NETZSCH 404 F1 Pegasus system. The DTA measurement was performed between room temperature and ~1300 K with a heating and cooling rate of 10 K min^{-1}. The maximum heating temperature for alloys rich in arsenic and arsenic selenides did not exceed 850 K, which does not exceed their sublimation and boiling temperatures. The device was previously temperature-calibrated. For this purpose, pure metals (indium, tin, bismuth, and zinc, antimony, silver and copper) provided by NETZSCH for this purpose with the appropriate certificates were used as standards. DTA of the synthesized alloys was carried out in evacuated and sealed ampoules made of transparent quartz glass with a height of 1.5-2 cm and a diameter of 0.5 cm. The mass of the samples was in the range of 50-100 mg. The free volume of the ampoules was minimal (no more than 0.3 cm^3), which ensured the constancy of the alloy composition during DTA measurement. Temperatures of thermal effects were taken mainly from the heating curves. NETZSCH Proteus Software was used for the evaluation of the DTA data.

The XRD analysis was performed on a Bruker D2 ADVANCE diffractometer, with $CuKa_1$ radiation at room temperature. XRD patterns were indexed by using TopasV3.0 software by Bruker.

Thermodynamic studies were conducted by measuring the EMF of concentration chains of

the following type

(-) Cu (s) | $Cu_4RbCl_3I_2$ (s) | (Cu-As-Se) (s) (+) (1)

Equilibrium alloys of the system under study were used as the right electrodes for type (1) circuits. The right electrodes were prepared by pressing annealed alloys ground into powder in the form of tablets with a diameter of ~8-10 mm and a thickness of 4-6 mm. The methodology for constructing of (1) type cells and conducting EMF measurements was similar to that in [33, 45, and 55].

3. Results and discussion

A complete, mutually consistent picture of phase equilibria in the Cu-As-Se system was obtained by processing the set of obtained experimental data using information from the literature on the boundary binary systems Cu-Se, Cu-As, and As-Se [56] as well as previously studied subsystems Cu_2Se-Cu_3AsSe_4-As_2Se_3, Cu–Cu_2Se–As, and Cu_2Se–Cu_3AsSe_4-Se [53–55].

3.1. Solid-phase equilibria in the Cu-As-Se system at 300 K

Solid-phase equilibria in the Cu-As-Se system were obtained in general by a joint analysis of the set of experimental data on annealed alloys, including the phase diagrams of border binary systems (Fig. 4).

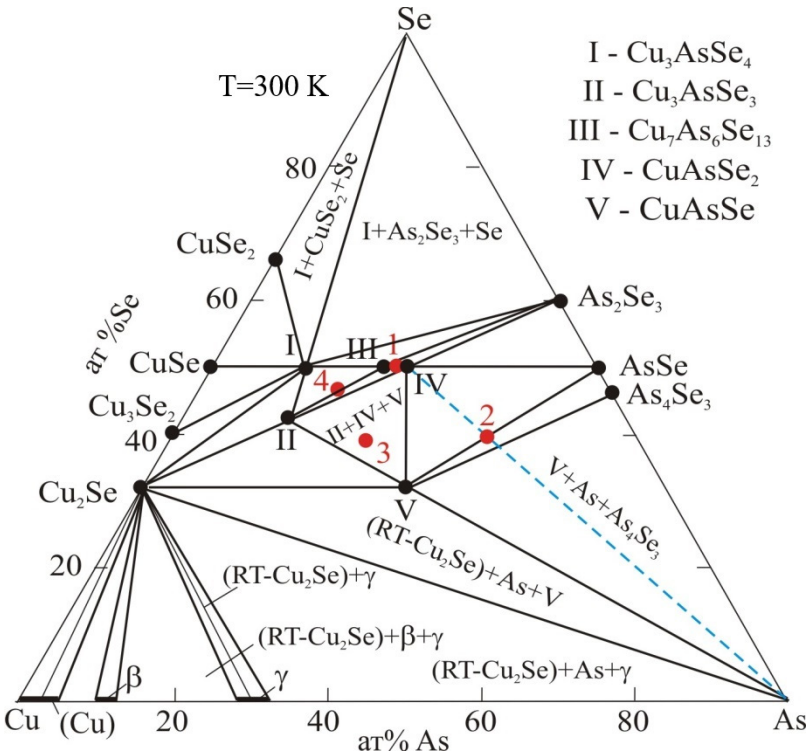

Fig. 4. Diagram of solid-phase equilibria of the Cu-As-Se system at 300 K

According to the constructed diagram, this system is characterized by the formation of 5 ternary compounds: Cu_3AsSe_4, Cu_3AsSe_3, $Cu_7As_6Se_{13}$, $CuAsSe_2$ and CuAsSe. Fig. 5 shows powder diffraction patterns of the indicated compounds. As can be seen, the synthesized samples of these compounds are single-phase and have diffraction patterns similar to those indicated in the literature [49-52]. The crystallographic data obtained from the powder diffraction patterns are presented in Table 2. A comparison of these data with those in the literature (Table 1) showed that they are in good agreement. The ternary compounds $Cu_6As_4Se_9$ and $Cu_4As_2Se_5$ (respectively, alloys 1 and 4 in Fig. 4) indicated in the literature have not been

confirmed by us. Their X-ray diffraction patterns (Fig. 6) consisted of sets of reflection lines of various compounds of this system.

Table 2. Crystal data of ternary compounds of the Cu-As-Se system

Compound	Structure, Sp.gr., lattice parameters; Å
α-Cu_3AsSe_4	Cubic, a=5.5347
β-Cu_3AsSe_4	Tetragonal, I-42m, a = 5.5295, c = 10.829
$CuAsSe_2$	Monoclinic, a = 5.116, b = 12.291, c = 9.467, $\beta = 98.55^0$
Cu_3AsSe_3	Cubic, Pm-3m, a = 5.7573
$Cu_7As_6Se_{13}$	Hexagonal, R3, a = 14.024, c = 9.613

Fig. 4 shows the tie lines related to the studied quasi-binary sections presented by us in [53-55]. The location of other connodes and three-phase regions is clearly established by the XRD studies (Fig. 6).

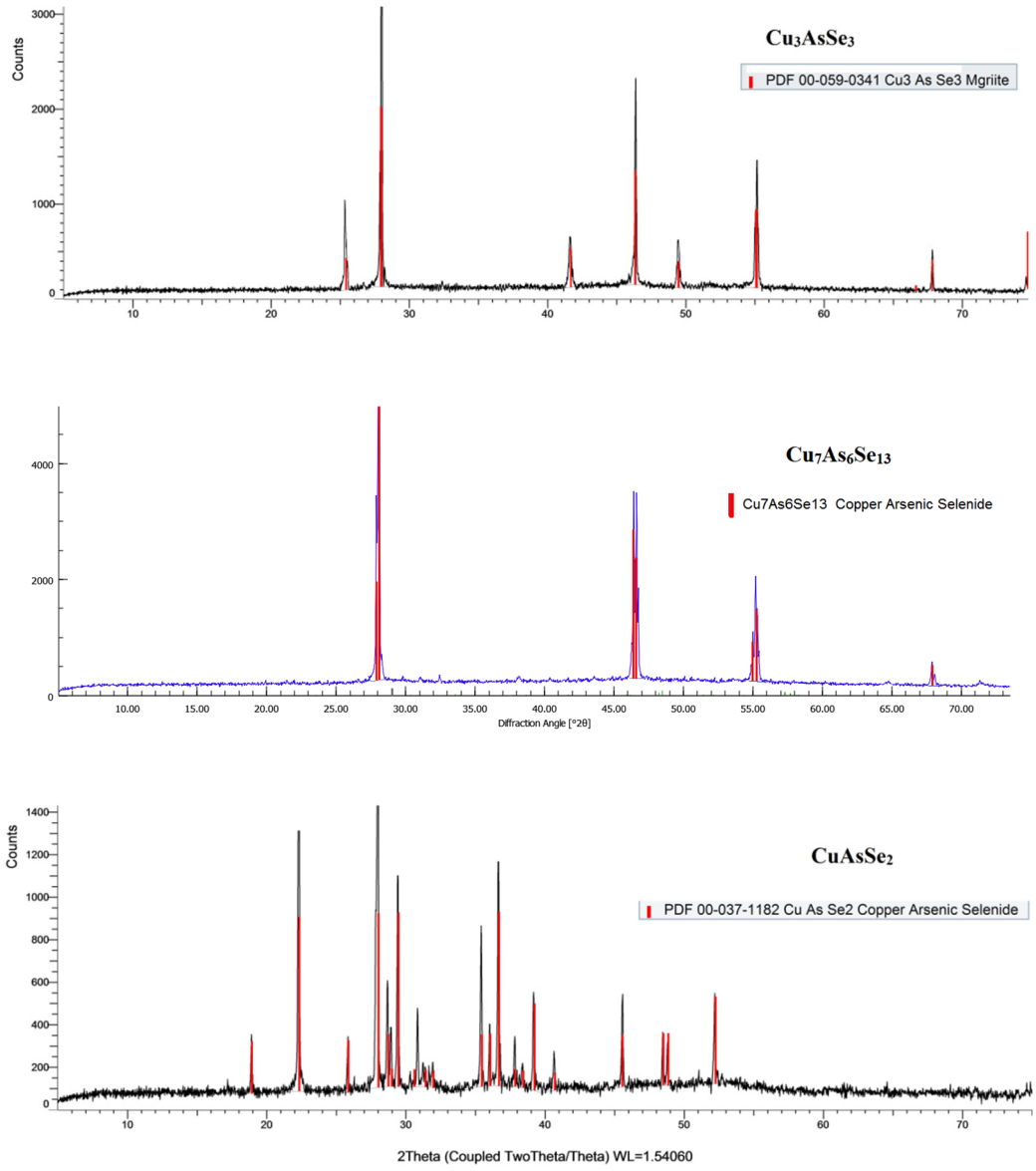

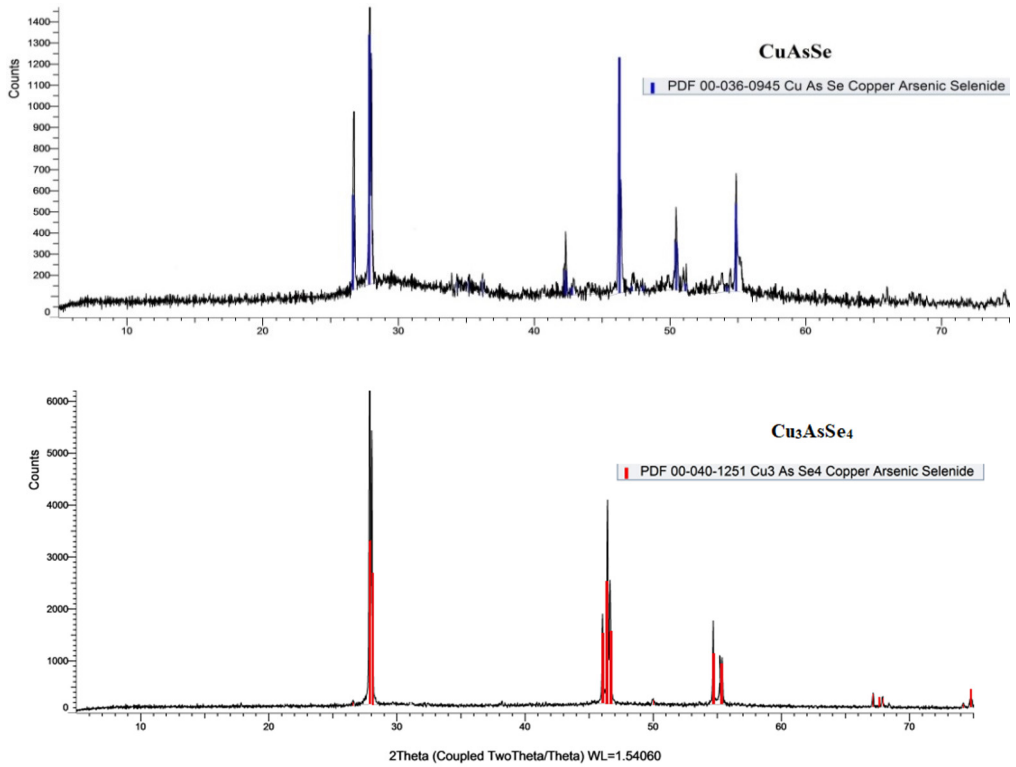

Fig. 5. Powder X-ray diffraction patterns of Cu_3AsSe_4, Cu_3AsSe_3, $Cu_7As_6Se_{13}$, $CuAsSe_2$ and CuAsSe compounds

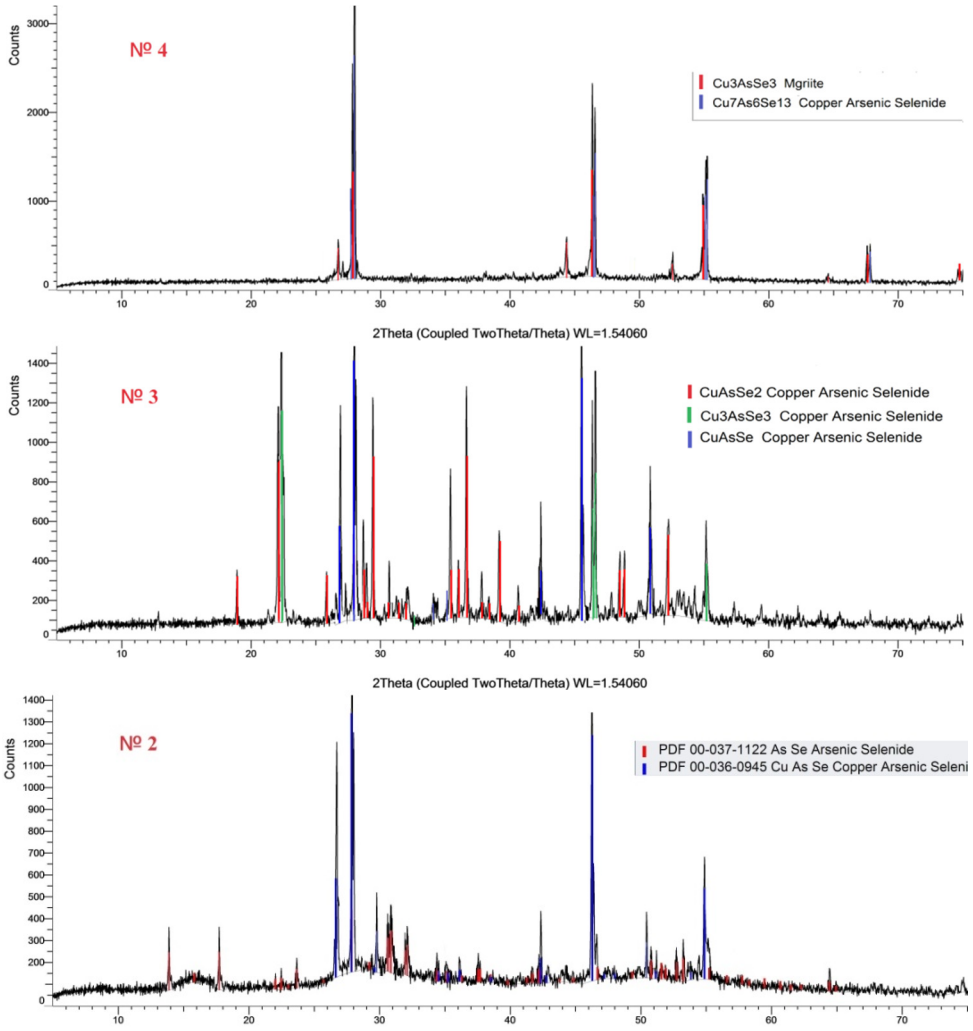

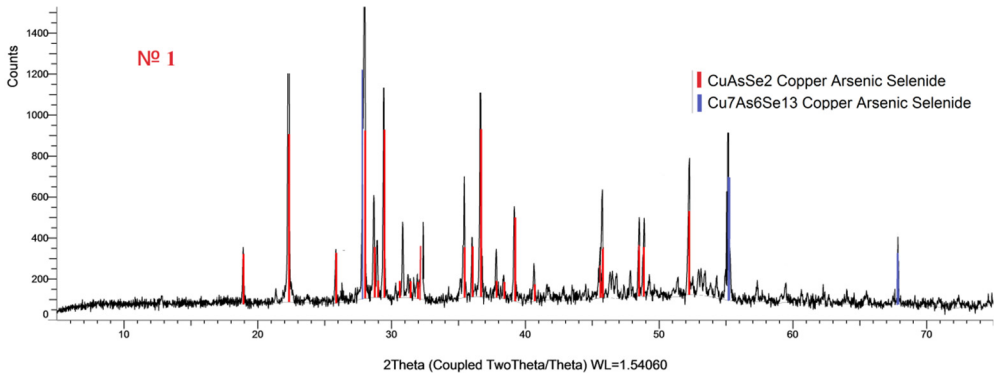

Fig. 6. Powder diffraction patterns of alloys 1, 2, 3, and 4 in Fig. 4

The isothermal section of the phase diagram in the region of Cu-Cu_2Se-As compositions (Fig. 4) consists of two independent triangles Cu-Cu_2Se-γ and γ-Cu_2Se-As. In this region, the presence of 3 three-phase regions delimited by tie-lines $(Cu_2Se)_I$-(Cu), $(Cu_2Se)_I$-Cu_8As (β) and $(Cu_2Se)_I$-γ was established. The presence of the first two-phase region is due to the fact that up to 6 at% As of solid solutions based on Cu are formed in the binary Cu-As system [56].

The compound $(Cu_2Se)_I$ also forms concentration tie-lines with the compounds Cu_3AsSe_4, Cu_3AsSe_3 and CuAsSe, as well as elemental arsenic.

In the distribution of phase regions, along with $(Cu_2Se)_I$, an important role belongs to the compounds Cu_3AsSe_4 and $CuAsSe_2$, which form tie-lines with the 8th and 6th phases of the system, respectively.

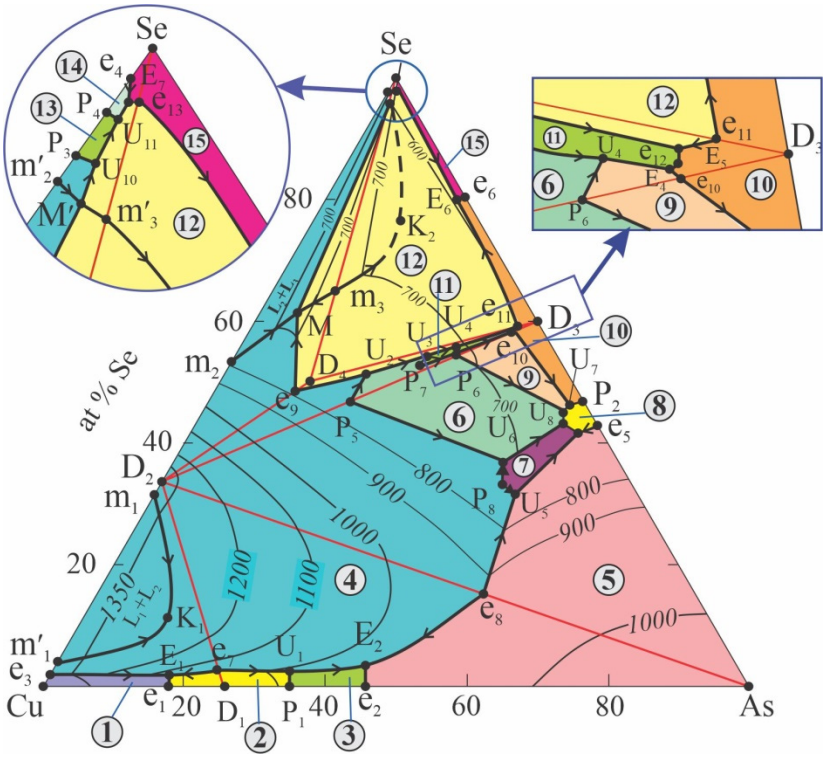

Fig. 7. Projection of the liquidus surface of the Cu-As-Se system. Fields of primary crystallization of phases: 1 - (Cu); 2 - γ; 3 - δ; 4 - (HT-Cu_2Se); 5 – As; 6 - Cu_3AsSe_3; 7 – CuAsSe; 8 – AsSe; 9 - $CuAsSe_2$; 10 – As_2Se_3; 11 - $Cu_7As_6Se_{13}$; 12 - Cu_3AsSe_4; 13 - (HT-CuSe); 14 - $CuSe_2$; 15 – Se

3.2. Liquidus Surface Projection. The liquidus surface projection of the Cu-As-Se system consists of 15 fields of primary crystallization of phases (Fig. 7). Five sections pertain to ternary copper-arsenic selenides, seven to binary compounds generated on the border systems, and three to the starting components. The fields of primary crystallization of the HT-

CuSe (P_3), $CuSe_2$ (P_4), and $Cu_7As_6Se_{13}$ (P_7) compounds are degenerate and are shown in Fig. 7 in an enlarged form (arbitrary scale).

The crystallization surfaces of (HT-Cu_2Se), As, Cu_3AsSe_4 and Cu_3AsSe_3 are most extended. The fields of primary crystallization (Cu), as well as γ (Cu_3As) and δ-phases of the binary Cu-As system extend along this side in the form of narrow stripes.

The T-x-y phase diagram of the Cu-As-Se system is characterized by the presence of two wide stratification regions L_1+L_2 and L_2+L_3 (L_1 is a metallic melt based on Cu-As; L_2 is a melt based on selenides; L_3 is a liquid phase rich in elemental selenium), formed by the penetration (or spread) of the corresponding regions on the Cu-Se boundary system.

The fields of primary crystallization of phases are delimited by numerous curves of monovariant equilibria and points of nonvariant equilibria. The coordinates of nonvariant points and the types of corresponding equilibria are given in Table 3.

Table 3. Non-variant equilibria in the Cu-As-Se system

Point in Fig.7	Equilibrium	T, K
D_1	L↔γ(Cu_3As)	1100
D_2	L↔(HT-Cu_2Se)	1403
D_3	L↔As_2Se_3	648
D_4	L↔I	750
P_1	L+γ ↔δ	982
P_2	L+As_2Se_3↔AsSe	570
P_3*	L+(HT-Cu_2Se) ↔(HT-CuSe)	650
P_4*	L+ (HT-CuSe) ↔$CuSe_2$	605
P_5	L+(HT-Cu_2Se) ↔II	770
P_6	L+II↔IV	725
P_7	L+II↔III	740
P_8	L+(HT-Cu_2Se)↔V	710
e_1	L↔(Cu)+γ	958
e_2	L↔δ+As	873
e_3	L↔(Cu)+(HT-Cu_2Se)	1335
e_4*	L↔ $CuSe_2$+Se	494
e_5	L↔As+AsSe	522
e_6	L↔As_2Se_3+Se	420
e_7	L↔(HT-Cu_2Se)+ γ	990
e_8	L↔(HT-Cu_2Se)+As	925
e_9	L↔(HT-Cu_2Se)+I	743
e_{10}	L↔IV+As_2Se_3	640
e_{11}	L↔ I+As_2Se_3	642
e_{12}	L↔ III+As_2Se_3	640
e_{13}	L↔I+Se	490
m_1(m_1´)	L_2↔L_1+(HT-Cu_2Se)	1373
m_2(m_2´)	L_2↔L_3+(HT-Cu_2Se)	796
m_3(m_3´)	L_2↔L_3+ I	713
U_1	L+γ↔(HT-Cu_2Se)+δ	965
U_2	L+(HT-Cu_2Se)↔I+II	720
U_3	L+II↔I+III	703

U_4	L+II↔III+IV	715
U_5	L+(HT-Cu_2Se)↔V+As	705
U_6	L+(HT-Cu_2Se)↔II+V	703
U_7	L+As_2Se_3↔ IV+AsSe	560
U_8	L+IV↔II+AsSe	545
U_9	L+II↔V+AsSe	530
U_{10}	L+(HT-Cu_2Se)↔I+(HT-CuSe)	630
U_{11}	L+(HT-CuSe)↔I+$CuSe_2$	600
M(M′)	L_2↔L_3+(HT-Cu_2Se)+I	690
E_1	L↔(Cu)+(HT-Cu_2Se)+γ	935
E_2	L↔(HT-Cu_2Se)+As+δ	855
E_3	L↔V+AsSe+As	515
E_4**	L↔III+IV+As_2Se_3	635
E_5**	L↔I+III+As_2Se_3	637
E_6	L↔I+As_2Se_3+Se	415
E_7	L↔I+$CuSe_2$+Se	490

* - *denotes equilibria degenerate at the angle Se of the concentration triangle*
** - *denotes equilibria degenerate at the points e_{10} and e_{12}.*

The eutectic curve emanating from point e_9 intersects the imiscibility region L_2+L_3 and transforms this equilibrium into a four-phase monotectic equilibrium (conjugate points M_1M_1' in Fig. 7).

In conclusion of this section, we note that the liquidus surface projection of this system obtained by us experimentally has a significantly more complex picture of phase equilibria compared to the liquidus surfaces projection given by the authors [48], which reflects only two ternary compounds Cu_3AsSe_4 and $CuAsSe_2$.

3.3. Some polythermal sections. The CuSe-AsSe section (Fig. 8) passes through the stoichiometric compositions of three ternary compounds of the Cu-As-Se system and is stable below the solidus, i.e. it does not cross three-phase regions. At high temperatures, from left to right, the section reflects the primary crystallization of the α-phase, HT-Cu_3AsSe_4, Cu_3AsSe_3, $CuAsSe_2$ and As_2Se_3.

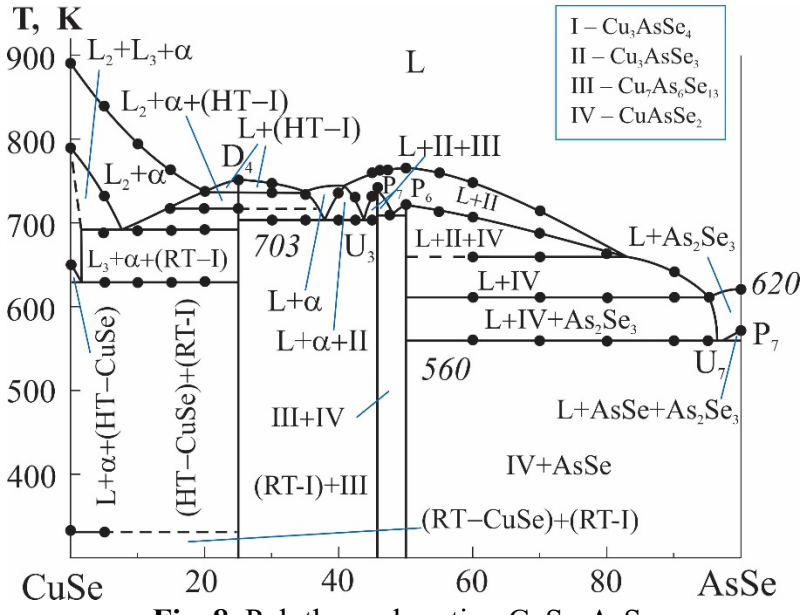

Fig. 8. Polythermal section CuSe-AsSe

In the composition range of 0-25 mol% AsSe, the monovariant eutectic reaction L↔α+HT- Cu_3AsSe_4 (Fig.7; curve e_9M) and monovariant monotectic reactions $L_2↔L_3+α$ (curve m_2M) and $L_2↔L_3$+RT-Cu_3AsSe_4 (curve m_3M) occur below the liquidus. The horizontals at 715, 695 and 630 K correspond, respectively, to the polymorphic transition of Cu_3AsSe_4, invariant monotectic (M) and transition (U_{10}) reactions (see Fig. 7 and Table 3). The thermal effects at 333 K correspond to the polymorphic transition of CuSe.

In the composition range of 25-50 mol% AsSe, a complex interaction is observed. This section intersects the eutectic e_9U_2 (L↔α+HT-Cu_3AsSe_4) and peritectic P_5U_2 (L+α↔Cu_3AsSe_3) curves. Crystallization is completed at 703 K by the transition reaction U_3 (Fig. 7 and Table 3). In a narrow composition range (43-50 mol% AsSe), crystallization continues by univariant peritectic reactions L+Cu_3AsSe_3↔$Cu_7As_6Se_{13}$ (curve P_7U_3 and P_7U_4) and L+Cu_3AsSe_3↔$CuAsSe_2$ (curve P_6U_4) and is completed by the invariant transition reaction U_4.

In the region of compositions >50 mol% AsSe, this section intersects the peritectic P_6U_8 and eutectic $e_{10}U_7$ curves. Crystallization is completed by the transition reaction U_7 (Table 3). Section 0.5CuSe-As (Fig. 9) intersects the fields of primary crystallization of two phases α and As. But below the liquidus, it reflects a number of invariant and monovariant reactions, which can be easily determined by comparing this section with Fig. 7 and Table 3. From left to right, crystallization is completed by the transition reactions U_{10}, U_2, U_6, and U_5. The horizontals at 405 and 385 K correspond to the polymorphic transition α↔α′ and the solid-state reaction α′+CuSe↔Cu_3Se_2, respectively.

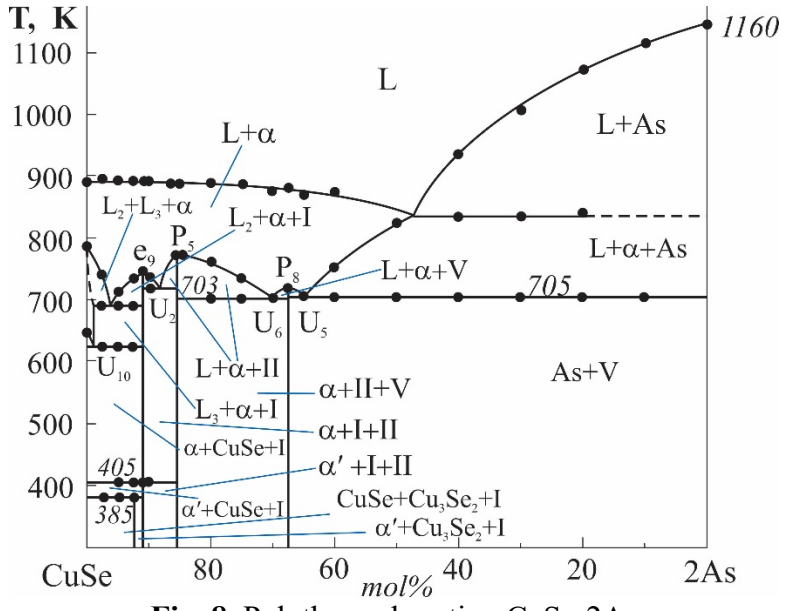

Fig. 8. Polythermal section CuSe-2As

Section $\frac{5}{3}$**CuSe$_2$-As$_2$Se$_3$** (Fig. 10) clearly demonstrates the nature of phase equilibria in the selenium-rich region of the system. It intersects the liquidus surfaces of the α-phase, Cu_3AsSe_4 and As_2Se_3. The α-phase completely and the Cu_3AsSe_4 compound partially crystallize from two stratified liquid phases according to the monovariant monotectic reactions m_2M ($L_2↔L_3+α$) and m_3M ($L_2↔L_3$+Cu_3AsSe_4). Then crystallization continues according to the invariant monotectic reaction at 680 K (Table 3, point M). The horizontals at 630, 600 and 490 K correspond to the transition reactions U_{10}, U_{11} and the eutectic equilibrium E_7, respectively.

In the region of compositions richer in As_2Se_3, the primary crystallization fields of Cu_3AsSe_4 and As_2Se_3 exhibit joint eutectic crystallization of these compounds (~35-93 mol% As_2Se_3), as well as eutectic mixtures of Cu_3AsSe_4+Se and As_2Se_3+Se. Crystallization is completed invariantly by the eutectic reaction E_6 (415 K).

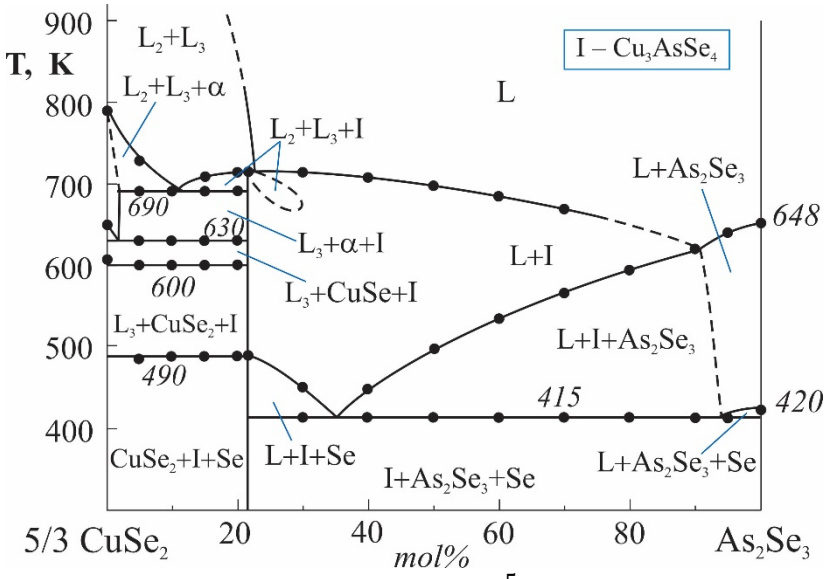

Fig. 10. Polythermal section $\frac{5}{3}$CuSe$_2$-As$_2$Se$_3$

It should be noted that the polythermal sections considered and the projection of the liquidus surface as a whole reflect the processes occurring during heating of samples brought to a state as close as possible to equilibrium by means of prolonged thermal annealing. When cooling the melts of these samples, especially from the region adjacent to arsenic selenides, they solidify in the form of glass or crystal+glass mixtures.

3.4. Thermodynamic properties of copper-arsenic selenides. Measurements of the EMF of reversible concentration chains of type (1) for equilibrium crystalline alloys of the Cu-As-Se system from the composition range Cu$_2$Se-CuAsSe-AsSe-Se led to reproducible results. According to the measurement data in each of the three-phase regions I+III+As$_2$Se$_3$, III+IV+As$_2$Se$_3$, I+II+III and IV+V+AsSe, indicated in the solid-phase equilibrium diagram of this system (Fig. 4), at a constant temperature the EMF has constant values regardless of the overall composition of the alloys, and undergoes abrupt changes when passing from one three-phase region to another. The data of EMF measurements of chains of type (1) for alloys from the three-phase region I+As$_2$Se$_3$+Se and the processing of their results were carried out by us in [55].

Fig. 11 shows the temperature dependences of the EMF of circuits of type (1) for a number of phase regions of the Cu-As-Se system. As can be seen, all these dependences are linear and can be used in thermodynamic calculations.

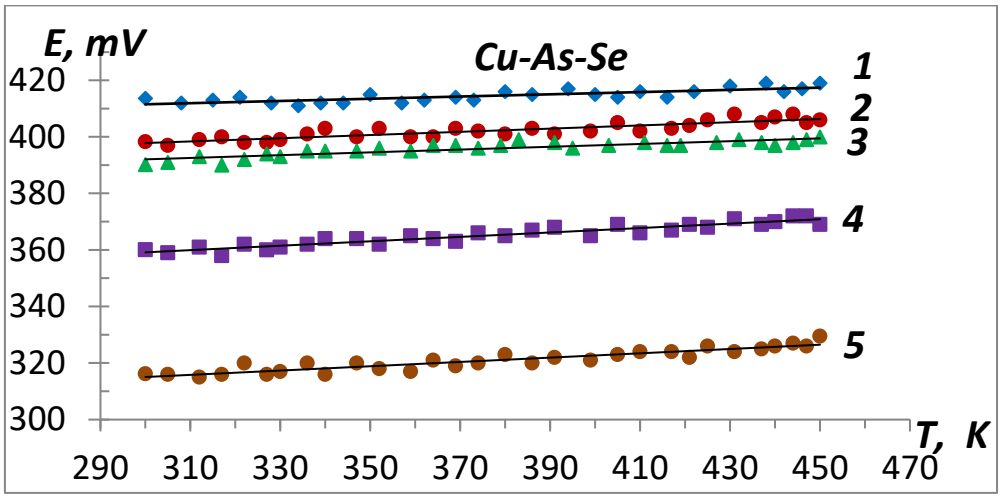

Fig. 11. Temperature dependences of the EMF of (1) type cells for alloys from phase areas I+As$_2$Se$_3$+Se (1) [55], I+III+As$_2$Se$_3$ (2), III+IV+As$_2$Se$_3$ (3), I+II+III (4) и IV+V+AsSe (5) of the Cu-As-Se system

For thermodynamic calculations, the results of EMF measurements in these phase regions were processed using the least squares method and linear equations of the type below were obtained

$$E = a + bT \pm t\left[\frac{S_E^2}{n} + S_b^2(T_i - \overline{T})^2\right]^{1/2}$$

Obtained equations are presented in Table 4. From the data in Table 4, the relative partial thermodynamic functions of copper in alloys at 298 K were calculated using known thermodynamic relationships (Table 5).

Table 4. Temperature dependences of the EMF of chains of type (1) in some phase regions of the Cu-As-Se system (T=300-450K)

The phase region in Fig. 4	E, мВ=a+bT±2S_E(T)
I+III+As_2Se_3	$382{,}92 + 0{,}0513T \pm 2\left[\frac{3{,}9}{30} + 6.2\cdot10^{-5}(T-376{,}8)^2\right]^{1/2}$
III+IV+As_2Se_3	$370.73 + 0{,}0652T \pm 2\left[\frac{2.4}{30} + 3.9\cdot10^{-5}(T-376.2)^2\right]^{1/2}$
I+II+III	$341.79 + 0{,}0601T \pm 2\left[\frac{2.7}{30} + 4.2\cdot10^{-5}(T-375.3)^2\right]^{1/2}$
IV+V+AsSe	$289.92 + 0{,}0879T \pm 2\left[\frac{3.2}{30} + 5.1\cdot10^{-5}(T-376.2)^2\right]^{1/2}$

According to the solid-phase equilibrium diagram of the Cu-As-Se system (Fig. 4), the values of partial molar quantities in the above-mentioned three-phase regions are thermodynamic characteristics of the following potential-forming reactions (all substances are crystalline):

$$2.2Cu + 1.6Cu_3AsSe_4 + 2.2As_2Se_3 = Cu_7As_6Se_{13}$$
$$Cu + Cu_7As_6S_{13} + As_2Se_3 = 8\ CuAsSe_2$$
$$Cu + \frac{1}{11}Cu_7As_6S_{13} + \frac{5}{11}Cu_3AsSe_4 = Cu_3AsSe_3$$
$$Cu + AsSe = CuAsSe$$

According to the equations of these reactions, the standard thermodynamic functions of formation and the standard entropies of copper-arsenic selenides can be calculated using the following relationships (ΔZ≡ΔG or ΔH):

$$\Delta Z^0_{Cu_7As_6Se_{13}} = 2.2\Delta\overline{Z}_{Cu} + 1.6\Delta Z^0_{Cu_3AsSe_4} + 2.2\Delta Z^0_{As_2Se_3}$$
$$\Delta Z^0_{CuAsSe_2} = 0.125\,\Delta\overline{Z}_{Cu} + 0.125\,\Delta Z^0_{Cu_7As_6Se_{13}} + 0.125\,\Delta Z^0_{As_2Se_3}$$
$$\Delta Z^0_{Cu_3AsSe_3} = \Delta\overline{Z}_{Cu} + \frac{1}{11}\Delta Z^0_{Cu_7As_6Se_{13}} + \frac{5}{11}\Delta Z^0_{Cu_3AsSe_4}$$
$$\Delta Z^0_{CuAsSe} = \Delta\overline{Z}_{Cu} + \Delta Z^0_{AsSe}$$

and the standard entropies:

$$S^0_{Cu_7As_6S_{13}} = 2.2(\Delta\overline{S}_{Cu} + S^0_{Cu}) + 1.6S^0_{Cu_3AsSe_4} + 2.2S^0_{As_2Se_3}$$

$$S^0_{CuAsSe_2} = 0.125(\Delta\overline{S}_{Cu} + S^0_{Cu}) + 0.125S^0_{Cu_7As_6Se_{13}} + 0.125S^0_{As_2Se_3}$$

$$S^0_{Cu_3AsSe_3} = \Delta\overline{S}_{Cu} + S^0_{Cu} + \frac{1}{11}S^0_{Cu_7As_6Se_{13}} + \frac{5}{11}S^0_{Cu_3AsSe_4}$$

$$S^0_{CuAsSe} = \Delta\overline{S}_{Cu} + S^0_{Cu} + S^0_{AsSe}$$

Table 5. Partial molar functions of copper in Cu-As-Se alloys at 298K

Phase area	$-\Delta\overline{G}_{Cu}$	$-\Delta\overline{H}_{Cu}$	$-\Delta\overline{S}_{Cu}$, J·K^{-1}·mole^{-1}
	κJ·mole^{-1}		
I+III+As_2Se_3	38,42±0,07	36,95±0,29	4,95±0,76
III+IV+As_2Se_3	37,65±0,05	35,77±0,23	6,29±0,61
I+II+III	34,71±0,06	32,98±0,24	5,80±0,64
IV+V+AsSe	30,50±0,06	27,97±0,26	8,48 ±0,69

In addition to our own experimental results (Table 4), the calculations used the values of the standard entropies of copper (33.15±0.08 J·K^{-1}·mole^{-1}) and selenium (42.13±2.09 J·K^{-1}·mole^{-1}) [59], as well as mutually consistent data sets for As_2Se_3 and AsSe (Table 5) [60].

Table 5. Standard thermodynamic functions of formation and standard entropies of ternary phases of the Cu-As-Se system

Compound	- $\Delta_fG°$ (298 K)	- $\Delta_fH°$ (298 K)	S° (298 K) J·K^{-1}·mole^{-1}
	κJ·mole^{-1}		
As_2Se_3 [60]	55,26±0,58	59,4±3,9	184,4±8,2
AsSe [60]	24,64±0,25	27,61±1,7	68,1±3,9
Cu_3AsSe_4 [55]	147.3±0.5	146.3±1.5	307±13
$Cu_7As_6Se_{13}$	441,8±2,3	446,1±11,7	970±27
$CuAsSe_2$	61.1±0.4	62.1±1.9	149.5±4.5
Cu_3AsSe_3	141,8±0,5	140,0±2,0	258,5±5,6
CuAsSe	55,1±0,3	55,6±2,0	109,5±4,7

Thus, using the EMF method with a Cu+-conducting solid electrolyte, new sets of thermodynamic data for copper-arsenic selenides were obtained, including the partial molar Gibbs free energy of formation, the enthalpy and entropy of copper in alloys and the corresponding standard thermodynamic functions of formation and standard entropies of ternary copper-arsenic selenides.

4. Conclusions

1. By employing powder X-ray diffraction and differential thermal analysis techniques to investigate carefully formed alloys by lengthy thermal annealing, along with information from the literature, a novel comprehensive picture of phase equilibria in the Cu-As-Se system was obtained.
2. We present and analyze the liquidus surface projection, the isothermal section at 300 K, and a few vertical phase diagram sections. The types and coordinates of monovariant and nonvariant phase equilibria were established.
3. It is established that the liquidus surface consists of 15 regions corresponding to the primary crystallization of three initial components, seven binary and five ternary compounds Cu_3AsSe_4, Cu_3AsSe_3, $Cu_7As_6Se_{13}$, $CuAsSe_2$ and CuAsSe.

4. The ternary compounds $Cu_6As_4Se_9$ and $Cu_4As_2Se_5$, indicated in the literature, have not been confirmed by us.
5. By measuring the EMF of the concentration circuits relative to the copper electrode and taking into account the diagram of solid-phase equilibria of the Cu-As-Se system, mutually consistent values of the standard thermodynamic functions of formation and standard entropies of the above-mentioned copper-arsenic selenides were obtained.

Acknowledgment

This work supported by the Azerbaijan Science Foundation – ***Grant No AEF-MCG-2022-1(42)-12/10/4-M-10****.*

References

1. Khan M.E., Aslam J. Metal-Chalcogenide Nanocomposites. Fundamentals, Properties and Industrial Applications. *Woodhead Publishing*. 2024, 265 p. DOI: 10.1016/C2022-0-00497-9
2. Basit A., Xin J., Murtaza G., Wei L., Hameed A., Guoyu W., Dai J.Y. Recent Advances, Challenges, and Perspective of Copper-Based Chalcogenides for Thermoelectric Applications. *EcoMat*. **Vol. 5(9)**, e12391. DOI: 10.1002/eom2.12391
3. Ivanchenko M., Jing H. Smart Design of Noble Metal–Copper Chalcogenide Dual Functional Nanostructures: Synthesis, Properties, and Applications**.** *Chemistry of Materials*. 2023, **Vol. 35(12)**, p. 4598–4620. DOI:10.1021/acs.chemmater.3c00346
4. Woodrow P. *Chalcogenides: Advances in Research and Applications*. New York: Nova Science Publishers. 2018. 111 p.
5. Scheer R., Schock H.W. *Chalcogenide Photovoltaics: Physics, Technologies, and Thin Film Devices.* Weinheim: Wiley-VCH. 2011. 384 p.
6. Maiti S., Maiti S., Khan A.H., Wolf A., Dorfs D., Moreels I., Schreiber F., Scheele M. Dye-Sensitized Ternary Copper Chalcogenide Nanocrystals: Optoelectronic Properties, Air Stability, and Photosensitivity. *Chemistry of. Materials.* 2019, **Vol. 31(7)**, p. 2443–2449. DOI:10.1021/acs.chemmater.8b05108
7. Khan M.M. *Chalcogenide-Based Nanomaterials as Photocatalysts. Amsterdam*: Elsevier. 2021. 376 p.
8. Ma S., Chen K., Qiu Y.H., Gong L.L., Pan G.M., Lin Y.J., Hao Z.H., Zhou L., Wang Q.Q. Controlled Growth of CdS-$Cu_{2-x}S$ Lateral Heteroshells on Au Nanoparticles with Improved Photocatalytic Activity and Photothermal Efficiency. *J. Mater. Chem. A*. 2019, **Vol. 7(7)**, p. 3408– 3414. DOI:10.1039/C8TA11154E
9. Kumar M., Meena B., Subramanyam P., Suryakala D., Subrahmanyam C. Emerging Copper-based semiconducting materials for photocathodic applications in solar driven water splitting. *Catalysts.* 2022, **Vol. 12(10)**, p. 1198. DOI:10.3390/catal12101198
10. Liu W.–D, Yang L., Chen Z.–G., Zou J. Promising and Eco–Friendly Cu_2X–Based Thermoelectric Materials: Progress and Applications. *Advanced Materials.* 2020, **Vol. 32(8)**, p. 1905703–28. DOI:10.1002/adma.201905703
11. Akhil S., Balakrishna R.G. $CuBiSe_2$ Quantum Dots as Ecofriendly Photosensitizers for Solar Cells. *ACS Sustainable Chemistry & Engineering Journal.* 2022, **Vol. 10(39)**, p. 13176-13184. DOI:10.1021/acssuschemeng.2c04333
12. Alonso-Vante N. *Chalcogenide Materials for Energy Conversion: Pathways to Oxygen and Hydrogen Reactions*. NewYork: Springer. 2018. 234 p. DOI: 10.1007/978-3-319-89612-0
13. Amrillah T., Prasetio A., Supandi A., Sidiq D., Putra F., Nugroho M., Salsabilla Z., Azmi R. Environment-friendly copper-based chalcogenide thin film solar cells: status and perspective. *Material Horizons*. 2023, **Vol. 10**, p. 313-339. DOI:10.1039/D2MH00983H
14. Viswanath A.K., Radhakrishna S. Copper Ion Conductors. *High Conductivity Solid Ionic Conductors*. 1989, p. 280-326. DOI:10.1142/9789814434294_0012
15. Nilges T., Pfitzner A. A structural differentiation of quaternary copper

argyrodites: structure – property relations of high temperature ion conductors. *Zeitschrift für Kristallographie - Crystalline Materials*. 2005, **Vol. 220(2-3)**, p. 281-294. DOI:10.1524/zkri.220.2.281.59142
16. Gorin Y.F., Mel'nikova N.V., Baranova E.R., Kobeleva O.L. Influence of ionic conductivity on the elastic characteristics of four-component copper and silver chalcogenides. *Technical Physics Letter*. 1997, **Vol. 23**, p. 550-552. DOI:10.1134/1.1261873
17. Centeno P., Alexandre M., Neves F., Fortunato E., Martins R., Águas H., Mendes M.J. Copper-Arsenic-Sulfide Thin-Films from Local Raw Materials Deposited via RF Co-Sputtering for Photovoltaics. *Nanomaterials*. 2022, **Vol. 12(19)**, p. 3268. DOI:10.3390/nano12193268
18. Yaroslavzev A.A., Kuznetsov A.N., Dudka A.P., Mironov A.V., Buga S.G., Denisov V.V. Laves polyhedra in synthetic tennantite, $Cu_{12}As_4S_{13}$, and its lattice dynamics. *Journal of Solid State Chemistry*. 2021, **Vol. 297(1)**, p. 122061. DOI:10.1016/j.jssc.2021.122061
19. Wei T.R., Qin Y., Deng T., Song Q., Jiang B., Liu R., Qiu P., Shi X., Chen L. Copper chalcogenide thermoelectric materials. *Sci. China Mater*. 2019, **Vol. 62(1)**, p. 8-24. DOI:10.1007/s40843-018-9314-5
20. Levinsky P., Candolfi C., Dauscher A., Tobola J., Hejtmánek J., Lenoir B. Thermoelectric Properties of the Tetrahedrite–Tennantite Solid Solutions $Cu_{12}Sb_{4-x}As_xS_{13}$ and $Cu_{10}Co_2Sb_{4-y}As_yS_{13}$ ($0 \leq x, y \leq 4$). *Phys. Chem. Chem. Phys*. 2019, **Vol. 21**, p. 4547–4555. DOI:10.1039/C9CP00213H
21. Hathwar V.R., Nakamura A., Kasai H., Suekuni K., Tanaka H.I., Takabatake T., Ibersen B.B., Nishibori E. Low-Temperature Structural Phase Transitions in Thermoelectric Tetrahedrite, $Cu_{12}Sb_4S_{13}$, and Tennantite, $Cu_{12}As_4S_{13}$. *Crystal Growth & Design*. 2019, **Vol. 19(7)**, p. 3979–3988. DOI:10.1021/acs.cgd.9b00385
22. McClary S.A., Li S., Yin X., Dippo P., Kuciauskas D., Yan Y., Baxter J.B., Agrawal R., Optoelectronic Characterization of Emerging Solar Absorber Cu_3AsS_4. *IEEE 46th Photovoltaic Specialists Conference (PVSC)*. 2019, p. 2310-2314. DOI:10.1109/PVSC40753.2019.8980590
23. Studenyak I.P, Molnar Z.R., Makauz I.I. Deposition and optical absorption studies of Cu–As–S thin films. *Semiconductor Physics, Quantum Electronics & Optoelectronics*. 2018, **Vol. 21(2)**, p. 167-172. DOI:10.15407/spqeo21.02.167
24. Ballow R.B., Miskin K.K., Abu-Omar M. Synthesis and Characterization of $Cu_3(Sb_{1-x}As_x)S_4$ Semiconducting Nanocrystal Alloys with Tunable Properties for Optoelectronic Device Applications. *Chemistry of Materials*. 2017, **Vol. 29 (2)**, p. 573-578. DOI:10.1021/acs.chemmater.6b03850
25. Pauporté Th., Lincot D., Electrical, optical and photoelectrochemical properties of natural enargite, Cu_3AsS_4. *Advanced Materials for Optics and Electronics*. 1995, **Vol. 5(6)**, p. 289-298. DOI:10.1002/amo.860050602
26. Mindat.org: *Open database of minerals, rocks, meteorites and the localities they come from*. Available at http://www.mindat.org
27. Filippou D., Germain P., Grammatikopoulos T. Recovery of Metal Values From Copper—Arsenic Minerals And Other Related Resources. *Mineral Processing and Extractive Metallurgy Review*. 2007, **Vol. 28(4)**, p. 247-298. DOI:10.1080/08827500601013009
28. Zhou S., Li T., Wang C., Tan Z., Guan X., Li H., Zhang W. Tennantite and Enargite Rejection in the Copper Flotation—A Mini-Review. *Journal of Minerals and Materials Characterization and Engineering*. 2023, **Vol. 11(3)**, p. 63-68. DOI:10.4236/jmmce.2023.113006
29. West D.R.F. *Ternary Phase Diagrams in Materials Science*. Boca Raton: CRC Press, 2013. 3rd edition. 240 p. DOI:10.1201/9781003077213
30. Babanly M.B., Mashadiyeva L.F., Babanly D.M., Imamaliyeva S.Z., Taghiyev D.B., Yusibov Y.A. Some issues of complex investigation of the phase equilibria and thermodynamic properties of the ternary chalcogenide systems by the EMF method. *Russian Journal Inorganic Chemistry*. 2019,

Vol. 64(13), p. 1649-1671. DOI:10.1134/S0036023619130035
31. Saka H. *Introduction To Phase Diagrams In Materials Science And Engineering*. London: World Scientific Publishing Company. 2020. 188 p. DOI:10.1142/11368
32. Mashadiyeva L.F., Babanly D.M., Poladova A.N., Yusibov Y.A., Babanly M.B. *Liquidus surface and phase relations in the Cu-Sb-S system. Properties and Uses of Antimony* – Editor: David J. Jenkins. *Nova Science Publishers*. 2022, p. 45-72. DOI:10.52305/OJKB5395
33. Mashadiyeva L.F., Mammadli P.R., Babanly D.M., Ashirov G.M., Shevelkov A.V., Yusibov Y.A. Solid-phase equilibrium in the Cu-Sb-S ternary system and thermodynamic properties of ternary phases. *JOM*. 2021, **Vol. 73(5)**, p.1522-1530. DOI:10.1007/s11837-021-04624-y
34. Babanly M.B., Mashadiyeva L.F., Imamaliyeva S.Z., Tagiev D.B., Babanly D.M., Yusibov Yu.A. Thermodynamic properties of complex copper chalcogenides (Review). *Chemical Problems*. 2024, **Vol. 22(3)**, p. 243-280. DOI:10.32737/2221-8688-2024-3-243-280
35. Bayramova U.R., Babanly K.N., Ahmadov E.I., Mashadiyeva L.F., Babanly M.B. Phase Equilibria in the Cu_2S-Cu_8SiS_6-Cu_8GeS_6 System and Thermodynamic Functions of Phase Transitions of the $Cu_8Si_{(1-x)}Ge_xS_6$ Argyrodite Phases. *Journal of Phase Equilibria and Diffusion*. 2023, **Vol. 44(3)**, p. 509–519. DOI:10.1007/s11669-023-01054-y
36. Bairamova U.R., Babanly K.N., Mashadieva L.F., Yusibov Yu.A., Babanly M.B. Phase Equilibria in the Cu_2Se-Cu_8SiSe_6-Cu_8GeSe_6 System. *Russian Journal of Inorganic Chemistry*. 2023, **Vol. 68(11)**, p. 1611–1621. DOI:10.1134/S0036023623602027
37. Mashadieva L.F., Alieva Z.M., Mirzoeva R.Dzh., Yusibov Yu.A., Shevel'kov A.V., Babanly M.B. Phase Equilibria in the Cu_2Se–$GeSe_2$–$SnSe_2$ System. *Russian Journal of Inorganic Chemistry*. 2022, **Vol. 67(5)**, p. 670–682. DOI:10.1134/S0036023622050126
38. Ismailova E.N., Mashadieva L.F., Bakhtiyarly I.B., Gasymov V.A., Gurbanova R.J., Mammadov F.M. Phase Equilibria in The Cu_2Se - Cu_3SbSe_4 - Cu_2SnSe_3 system. *Chemical Problems*. 2025, **Vol. 23(1)**. p. 36-46. DOI:10.32737/2221-8688-2025-1-36-46
39. Ismailova E.N., Mashadiyeva L.F., Bakhtiyarly I.B., Babanly M.B. Phase equilibria in the Cu_2SnSe_3–Sb_2Se_3–Se system. *Condensed Matter and Interphases*. 2023, **Vol. 25(1)**, p. 47–54. DOI:10.17308/kcmf.2023.25/10973
40. Babanly M.B., Mashadieva L.F., Imamaliyeva S.Z., Babanly D.M., Taghiyev D.B., Yusibov Y.A. Complex copper-based chalcogenides: a review of phase equilibria and thermodynamic properties. *Condensed Matter and Interphases*. 2024, **Vol. 26(4)**, p. 579-619. DOI:10.17308/kcmf.2024.26/12367
41. Alverdiyev I.J., Aliev Z.S., Bagheri S.M., Mashadiyeva L.F., Yusibov Y.A., Babanly M.B. Study of the $2Cu_2S+GeSe_2 \leftrightarrow Cu_2Se+GeS_2$ reciprocal system and thermodynamic properties of the $Cu_8GeS_{6-x}Se_x$ solid solutions. *Journal of Alloys and Compounds*. 2017, **Vol. 691**, p. 255-262. DOI:10.1016/j.jallcom.2016.08.251
42. Gasanova Z.T., Mashadieva L.F., Yusibov Y.A., Babanly M.B. Phase equilibria in the Cu_2S–Cu_3AsS_4–S system. *Russian Journal of Inorganic Chemistry*. 2017, **Vol. 62(5)**, p. 591–597. DOI:10.1134/s0036023617050126
43. Ismayilova E.N., Mashadiyeva L.F., Bakhtiyarly I.B., Babanly M.B. Phase equilibria in the Cu_2Se–SnSe–Sb_2Se_3 system. *Azerbaijan Chemical Journal*. 2022, **no. 1**, p. 73-82
44. Gasanova Z.T. Mashadieva L.F. Yusibov Yu.A., Babanly M.B. Phase equilibria in the Cu–Cu_2Se–As system. *Russ. J. Inorg. Chem*. 2017, **Vol. 62**, p. 598–603. DOI:10.1134/S0036023617050151
45. Mashadiyeva L.F., Babanly D.M., Hasanova Z.T., Yusibov Yu.A., Babanly M.B. Phase Relations in the Cu-As-S System and Thermodynamic Properties of Copper-Arsenic Sulfides. *J. Phase Equilib. Diffus*. 2024, **Vol. 45**, p. 567-582 DOI:10.1007/s11669-024-01115-w
46. Babanly M.B., Yusibov Yu.A., Abishev V.T. *Ternary Chalcogenides Based on*

Copper and Silver. Baku: Bakinsk. Gos. Univ., 1993. 342 P. [in Russian].
47. Tédenac J.-C. *Arsenic–Copper–Selenium. In: Ternary Alloys* / Ed. by G. Petzow, G. Effenberg, and F. Aldinger. *VCH, Weinheim*. 1994. V. **10**, p. 129–134.
48. Cohen K., Rivet J., Dugué J. Description of the Cu-As-Se ternary system. *Journal of Alloys and Compounds*. 1995, **Vol. 224(2)**, p. 316–329. DOI:10.1016/0925-8388(95)01534-5
49. Golovei M.I., Golovei M.I., Voroshilov Y.V., Potorii M.V. Investigation of the systems C(Ag,Tl)-B^5-Se. *Izv. Vyssh. Uchebn. Zaved., Khim. Khim. Tekhnol.*, 1985, **Vol. 28**, p. 7–11.
50. Blachnik R., Kurz G. Compounds in the system Cu_2Se-As_2Se_3. *Journal of Solid State Chemistry*. 1984, **Vol. 55**, p. 218-224.
51. Majid C.A., Hussain M.A. Crystal data for ternary compounds of the system Cu-As_2Se_3. *Journal Applied Crystallography*. 1987, **Vol. 20**, p. 323.
52. Takeuchi Y., Horiuchi H. The application of the partial Patterson method and the thirteenfold hexagonal superstructure of $Cu_7As_6Se_{13}$. *Zeitschriftfür Kristallographie – Crystalline Materials*. 1972, **Vol. 135**, p. 93–119.
53. Mashadiyeva L.F., Hasanova Z.T., Yusibov Yu.A., Babanly M.B. Phase equilibria in the Cu_2Se–Cu_3AsSe_4 –As_2Se_3 system. *Azerbaijan Chemical Journal.* 2024, **no. 3**, p. 83-93. DOI:10.32737/0005-2531-2024-3-83-93
54. Mashadieva L.F., Gasanova Z.T., Yusibov Y.A., Babanly M.B. Phase equilibria in the Cu–Cu_2Se–As system. *Russian Journal of Inorganic Chemistry*. 2017, **Vol. 62(5)**, p. 598–603. DOI:10.1134/s003602361705015
55. Mashadieva L.F., Gasanova Z.T., Yusibov Yu.A., Babanly M.B. Phase Equilibria in the Cu_2Se–Cu_3AsSe_4–Se System and Thermodynamic Properties of Cu_3AsSe_4. *Inorganic Materials*. 2018, **Vol. 54(1)**, p. 8–16. DOI:10.1134/s0036023619060093
56. Ed. T.B. Massalski. *Binary alloy phase diagrams* 2nd edition. Ohio: ASM International, Materials park. 1990. 3589 p.
57. Vinogradova G.Z. *Glass Formation and Phase Equilibria in Chalcogenide Systems*, Moscow: Nauka. 1984. 173 p. (*In Russian*)
58. Tanaka K. *Chalcogenide Glasses*. *Encyclopedia of Materials: Science and Technology*. 2001, p. 1123-1131. DOI:10.1016/B978-0-12-803581-8.02338-9
59. Yorish V.S., Yungman V.S. Ed. *Thermal Constants of Substances Database*. 2006. http://www.chem.msu.su/cgi-bin/tkv
60. Babanly D.M., Velieva G.M., Imamaliyeva S.Z., Babanly M.B. Thermodynamic functions of arsenic selenides. *Russ. J. Phys. Chem.* 2017, **Vol. 91**, p. 1170–1173. DOI:10.1134/S0036024417070044